A glassy carbon electrode modified by a triply-fused-like Co(ii) polyporphine and its ability for sulphite oxidation and detection

Sébastien D Rolle, Charles H. Devillers, Sophie Fournier, Olivier Heintz, Hervé Gibault, Dominique Lucas

NJC

PAPER

A glassy carbon electrode modified by a triply-fused-like Co(II) polyporphine and its ability for sulphite oxidation and detection

Received 00th January 20xx,
Accepted 00th January 20xx

DOI: 10.1039/x0xx00000x

www.rsc.org/

Sébastien D. Rolle,[a] Charles H. Devillers,*[a] Sophie Fournier,[a] Frédéric Herbst,[b] Olivier Heintz,[b] Hervé Gibault[c] and Dominique Lucas*[a]

This article presents a conducting Co(II) polyporphine polymer easily and rapidly obtained (less than 2h30) on the surface of a glassy carbon electrode from the transformation of an initial Mg(II) porphine solution in a four step process (including electrochemical and chemical stages). The intimate molecular structure is argued on the basis of the electrochemical response of the modified electrode, as well as its surface characterization. Thanks to its apparent stability in water over potential cycling and its high density in active Co(II) centers, the electrosynthesized film demonstrates its ability to catalyze sulphite oxidation in aqueous solutions.The mechanism of this molecular catalysis was assessed through specifically designed voltammetric experiments. The performances of this system as an analytical method for sulphite determination in water were also evaluated (linearity, limits of detection and quantification).

Introduction

Sulphite is a common additive in foods and wine.[1-3] Due to its antioxidizing properties, this compound contributes to the conservation of the product and exerts a protective action on its taste. Apart from this positive role sulphite is also a recognized allergen and can provoke health troubles which gravity varies from minor (headache, urticarial) to severe (edema, respiratory disease).[3-8] Therefore official methods for sulphite quantification are available.[9, 10] Nevertheless, these methods are long to operate and suffer from a relatively poor accuracy (especially for low sulphite concentration levels). Other analytical methods providing high precision results have been described using ICP-MS,[11] ion chromatography[12, 13] or capillary electrophoresis.[14, 15] But these instrumental techniques have important running costs, need qualified operators and remain time consuming. This situation has motivated the recent development of electrochemical sensors for sulphite analysis.[16-27] Advantageously these devices are easy to use and are able to deliver almost immediate results. Most usually these systems incorporates a molecular catalyst which facilitates the electrochemical transformation of the sulphite ion at the electrode surface and therefore favours the emission of the current signal.

Porphyrin based materials are adequate for catalyzing sulphite oxidation,[28-30] especially in the Co(II) complex form.[31, 32] In the reported studies, the catalytically active porphyrin molecule is dispersed in solution,[31] or deposited on the electrode surface, through drop casting,[29, 30] or by electropolymerization.[30-33] In this last case, a polymerizable function must be implanted at the periphery of the macrocycle at the stage of the monomer. The resulting molecule is more voluminous thus causing a limitation in density of catalytical sites of the ultimate material which can be detrimental to sensitivity. In our previous work,[34] we described an efficient process to obtain a Co(II) polyporphine film of type I (**pCoP-I**), *i.e.* a *meso-meso*-linked Co(II) porphine polymer, on the working electrode.[35] Due to the absence of any substituent and the direct linkage between porphine units, this new material is expected to exhibit a particularly high density of metallic centers which could provide superior capacities in electrocatalysis.

Thus, this article deals with the oxidative transformation of pCoP-I into Co(II) polyporphine of type II (**pCoP-II**), *i.e.* a triply-fused-like porphine polymer. Contrary to pCoP-I, this material exhibits a stable electrochemical response in aqueous media, which is a required condition for a use in a sensor. Besides the electrochemical study, this polymer has also been characterized by spectroscopic (XPS, SEM-EDX) measurements. Moreover, the ability of pCoP-II to catalyze sulphite oxidation has been demonstrated. Experiments on rotating disk electrode were also carried out to address the mechanism of the electrochemical process. Finally, the performances of the pCoP-II modified electrode for sulphite detection and quantification in water were evaluated.

Experimental

Reagents, materials and methods

The MgP monomer was synthesized following Lindsey's procedure.[36] It was ultimately purified according to Devillers *et al.*[37]

[a] *Institut de Chimie Moléculaire de l'Université de Bourgogne (ICMUB), CNRS UMR 6302, Université de Bourgogne Franche-Comté, 21078 Dijon, France*
[b] *Laboratoire Interdisciplinaire Carnot de Bourgogne (ICB), UMR CNRS 5209, Université de Bourgogne Franche-Comté, 21078 Dijon, France*
[c] *Institut Œnologique de Champagne (IOC), 7 rue Aristide Briand, 21700 Nuits-Saint-Georges, France*
Authors to whom correspondence should be addressed (e-mail): Dr. C.H. Devillers (charles.devillers@u-bourgogne.fr); Pr D. Lucas (dominique.lucas@u-bourgogne.fr)

Acetonitrile (AN) was HPLC grade (Prolabo) and was distilled over CaH_2 under Ar. Dimethylformamide (DMF) was purchased from Carlo Erba (HPLC Grade). Tetra-*n*-butylammonium hexafluorophosphate ($TBAPF_6$) was synthesized by mixing stoichiometric amounts of tetra-*n*-butylammonium hydroxide (Alfa-Aesar, 40% w/w aq soln) and hexafluorophosphoric acid (Alfa-Aesar, *ca*. 60% w/w aq soln). After filtration, the salt was recrystallized three times in ethanol and dried at 110 °C during at least 2 days. $Co(OAc)_2.4H_2O$ was purchased from Carlo Erba.

A 1 M aqueous sulphite solution was prepared from sodium sulphite Na_2SO_3 (Prolabo pur 98+%). For sulphite detection studies, fixed amounts of this initial solution were added using automatic Thermo Fisher pipette.

Electrochemical measurements (film deposition and its characterization in the monomer-free solution) were performed in AN under an Ar atmosphere in a three-electrode glass cell. Working electrodes (WE) were Pt and glassy carbon (GC) disks with surface areas of about 0.03 (Pt) and 0.07 (GC) cm². For XPS and SEM measurements, glassy carbon plates (25x5x3 mm) purchased from Alfa Aesar were used as WE. A Pt wire was used as counter electrode (CE). A saturated aqueous calomel (SCE) was used as reference electrode (RE). The RE was separated from the WE compartment by a double frit comprising an intermediate background solution (0.1 M $TBAPF_6$ + AN). All the potentials in this manuscript are indicated vs. SCE.

All the electrochemical studies were realized using Autolab PGSTAT 302N potentiostat. All potentiodynamic experiments (CV) (for measuring redox responses of films) were performed at the scan rate of 100 mV/s unless otherwise noted.

Electrochemical measurements in aqueous media were performed in sodium nitrate 0.1 M solution ($NaNO_3$, Acros Organics, 99+% for analysis) in distilled water under Ar atmosphere in a three-electrode glass cell. As previously, CE was a platinum wire and RE was SCE. The RE was separated from the WE compartment by a double frit comprising an intermediate background solution (0.1 M $NaNO_3$ in distilled water).

For studies on rotating disk electrode, a Radiometer Analytical EDI101 in association with a Radiometer Analytical CTV101 control unit was used.

pH measurements were realized with Radiometer Analytical pH meter PHM 210.

XPS measurements were performed with the use of SIA100 device (Cameca Riber apparatus) with non-monochromatized Al Kα source (1486.6 eV). SEM imaging accompanied by EDX analysis was performed with scanning electronic microscope JEOL JSM6400F equipped by Oxford Instruments EDS analyzer.

Material synthesis procedures

The initial polymeric films of magnesium(II) porphine were deposited by potentiostatic polymerization at 0.65 V in a polymerization bath containing 0.5 mM of MgP and 1.5 mM of 2,6-lutidine in $TBAPF_6$ 0.1 M in AN.[38] The polymerization was automatically stopped when the deposition charge reached 10 mC/cm².

To remove Mg(II) in the polymers, electrodes coated with pMgP-I were carefully rinsed with AN and placed during 5 to 60 min (see below) in a 0.01 M hydrochlorhydric acid (HCl) solution in AN under Ar atmosphere at room temperature. Then, the films were rinsed with a 2.5% NH_3 solution in AN to recover the free base form (pH_2P-I, see below) and they were finally rinsed with AN for further studies. To insert Co(II) in the porphine macrocycle, pH_2P-I modified electrodes were dipped in a cobalt(II) acetate saturated solution in DMF and warmed at 110 °C during 30 min under Ar. These pCoP-I films were then carefully rinsed with distilled H_2O and AN before characterization.

pCoP-II was synthetized by pCoP-I film oxidation. 20 cycles in 0.1 M $TBAPF_6$ in AN between -1.8 and 1.4 V were needed to ensure the complete transformation. See below for more information.

Results and discussion

Previously to this work, we reported the electrochemical synthesis and characterization of magnesium polyporphine films.[35] The reaction proceeds through the oxidation of monomeric magnesium porphine (**MgP**) and two distinct forms of polymer are obtained depending on the applied potential (Scheme 1). The so-called **type I** polymer is formed at low potential (below 0.65 V), whereas applying a higher potential (> 0.65 V) leads to the **type II** compound The molecular structure differs fundamentally between the two polymer types. Indeed, polyporphine of type I is characterized by a single *meso-meso* bond between the monomer units. On the other hand, polyporphine of type II contains three different bonds between the elemental units: two *β-β* and one *meso-meso* bonds. As a consequence, the two polymers present different electrochemical properties. If pMgP-I behaves as a semiconductor, pMgP-II appears conductive on all the potential measurement window.

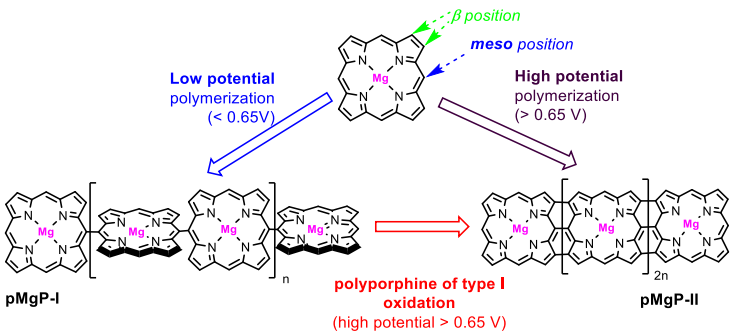

Scheme 1. Routes to obtain the different magnesium(II) polyporphine structures. Type I (pMgP-I) and type II (pMgP-II) polymers are represented on the left side and the right side, respectively. Adapted from

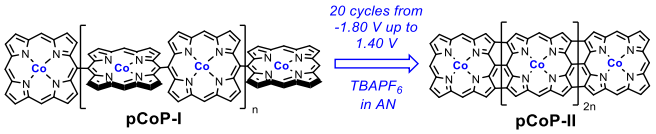

Scheme 2. Synthetic procedure to obtain pCoP-II film from the initial pCoP-I polymer

In our previous contribution in this field[34, 39] we demonstrated that the magnesium(II) centers in pMgP-I could be exchanged with a cobalt(II) ion thus providing an easy, quick and repeatable way to obtain a cobalt(II) polyporphine of type I pCoP-I. Since this time we experienced that this material was unstable in aqueous matrix over potential cycling although it was designed for a use in electrochemical sensing in this medium. Therefore, starting from pCoP-I, we intended to make directly the conversion into the presumably more stable type II polymer. As expected this reaction proceeds well by electrochemical oxidation in acetonitrile. Practically the transformation is achieved in 20 minutes through 20 successive voltammetric cycles between -1.80 and +1.40 V vs. SCE (Scheme 2).

Electrochemical response of Co(II) polyporphine in organic media

Fig. 1 shows the evolution of the cyclic voltammogram of the Co(II) polyporphine film during the course of pCoP-II synthesis. All the different peaks are identified and their characteristics are gathered in Table 1.

As explained in our previous work,[34] in pCoP-I, the peak system O1/R1 around 0.4 V can be attributed to the Co(II)/Co(III) redox couple. The O1 signal mainly arises from the oxidation of all Co(II) ions into the Co(III) state but it also contains a parasite contribution called prepeak. Prepeaks (like signal P in reduction) come from the residual discharge of the conducting polymer after it has been submitted previously to oxidation or reduction. This phenomenon is conditioned by the resistive behavior of pCoP-I between -0.5 V and 0.1 V. This non-conductive interval is responsible for the incomplete discharge of the polymer during the cycle and explain prepeaks appearance at its limit values.[34, 40-44]

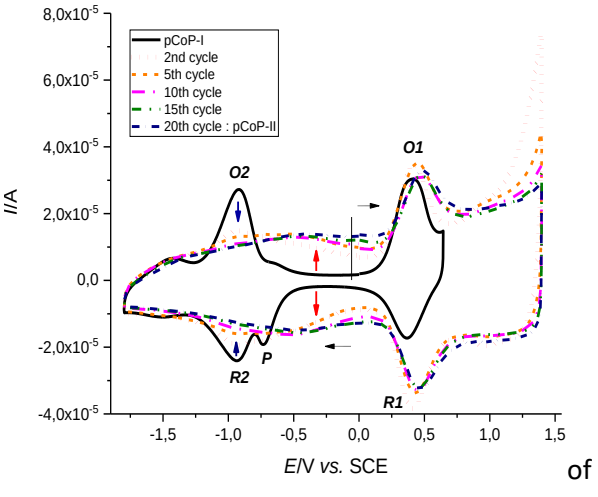

Fig. 1. Cyclic voltammograms ($TBAPF_6$ 0.1 M in AN, v = 0.1 $V.s^{-1}$) of Co(II) polyporphine film deposited on GC disc during the transformation from pCoP-I in pCoP-II. Black solid line: voltammogram corresponding to the initial pCoP-I film. Dark blue dashed-dotted line: CV obtained on the 20th cycle and corresponding to the pCoP-II full signal.

Table 1. Relevant parameters for peaks displayed on **Fig. 1** (films deposited on GC disk, AN 0.1 M $TBAPF_6$, v = 0.1 $V.s^{-1}$). *N.D.* means that the peaks could not be identified on the CV.

	Characteristic signal	O1	02	R1	R2	P	O1/R1 ratio
pCoP-I	Peak potential (V)	0.41	-0.92	0.37	-0.93	-0.73	
	Charge (µC)	5.1	5.3	-4.5	-5.4	-0.6	1.13
	Peak intensity (µA)	30.4	27.3	-17.3	-24.0	-19.2	
pCoP-II (20th cycle)	Peak potential (V)	0.48		0.47			
	Charge (µC)	5.0	*N.D*	5.0	*N.D.*	*N.D*	1.00
	Peak intensity (µA)	33.0		-32.2			

On the other hand, signals R2 and O2 around -0.9 V are attributed respectively to the reduction of Co(II) in Co(I) and to the reverse oxidation of Co(I) in Co(II).[45]

At first, the change of pCoP-I in pCoP-II is characterized by an important increase of capacitive current between -0.5 V and 0.1 V as outlined in Fig. 1. For example, at -0.3 V, the baseline current increases by more than a factor 8 (pCoP-I: 1.64 µA; pCoP-II: 13.7 µA). This increase is illustrated by red arrows on Fig. 1. As reported earlier[35, 46] and supported by some theoretical studies[47] for the magnesium(II) analogous materials, this evolution witnesses an evolution in the mechanism of electron transport inside the film.

It should be underlined that the O1/R1 system is kept in the transformation to the type II material (see Fig. 1 and Table 1). Slight shifts of the peak potentials are noted (+10 and +50 mV for O1 and R1, respectively), which potentially has two origins: 1) the variation of the normal potential associated to Co(II) → Co(III) reaction as this parameter is related to the fine molecular structure of the porphyrin unit; 2) the disappearance of the pre-peak (see above) which also certainly influences the peak position.

Table 1 gathers the charge values associated with O1 and R1 at the type I and II levels as deduced from the peak integration versus time. First of all, both materials have nearly the same value for O1 which seems to indicate that the transformation to p-CoP-II does not affect the content in cobalt. At the stage of p-CoP-II, R1 has exactly the same area as O1 (O1/R1 charge ratio = 1.00) meaning that this electrode process is fully reversible. The case is different for p-CoP-I for which R1 has significantly lost in surface comparatively to O1 (O1/R1 charge ratio = 1.13), that is in accordance with the polymer undergoing the reaction of Scheme 2 over oxidation. Finally, it should be stressed that the R2/O2 peak system progressively disappears during the evolution to type II, which is presently unexplained.

of

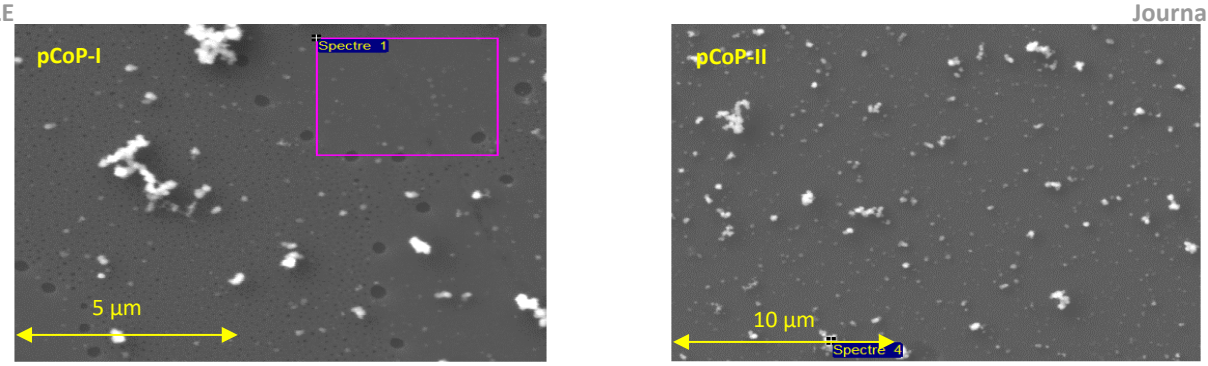

Fig. 2. SEM photographs for the cobalt(II) polyporphine of type I (left) and type II (right). The dimension scales are indicated by the yellow double-arrows in the left bottom corner.

SEM and XPS characterization of pCoP-II

For a more convenient observation in Scan Electron Microscopy (SEM) and X-Ray Photoelectron Spectroscopy (XPS) the electropolymerization and subsequent transformation to the cobalt(II) materials were carried out on GC plates. The same conditions as on GC disk were used, with in particular the polymer deposition being stopped for a charge of 10 mC/cm^2. Three samples of each polymer (pCoP-I and pCoP-II) were synthesized. No discrepancy of results was noticed between them.

Fig. 2. displays representative pictures of pCoP-I and pCoP-II. The two compounds present a very close aspect. In both cases the film is composed in the background of a uniform layer over which agglomerates of polymeric particles (individual size < 1 µm) have grown. As previously established, this particular morphology is generated when the magnesium polyporphine films are formed on the electrode surface.[38] The pictures of Fig. 2 demonstrate that this morphology is essentially unaffected by the treatment leading to pCoP-II. The conversion to pCoP-II is no more influent in spite of the profound change in the molecular structure induced by cross-linking between the porphyrin units. EDX analyses have been undertaken at different points of the deposit: the composition (Co and N content) is found uniform whatever is the sampled area.

Finally, dark circles in the 300-400 nm range are also visible in the left image of Fig. 2. They are attributed to pores which are formed in the background layer when the modified GC plates are submitted to vacuum for drying.

In order to acquire more information about the elemental composition of the different pCoP films, X-ray photoelectron spectroscopy (XPS) measurements were made on modified GC plate. XPS spectra focused on the Co 2p energy region of pCoP-I and pCoP-II are shown in Fig. 3.

For the response of cobalt (Fig. 3), peaks at 780.3 eV and 796.0 eV are obtained for the Co $2p_{3/2}$ and Co $2p_{1/2}$ spin states, respectively. These values are comparable with previous XPS studies of Co(II) in porphyrin derivative materials.[48-51] Moreover, no difference in peak values could be observed in the Co 2p signals between pCoP-I and pCoP-II. That means that no Co chemical form transformation occurs during the pCoP-II synthesis from pCoP-I. Cobalt in pCoP-II keeps its oxidation level +2.

Conversely, a clear evolution is noted for the N 1s response between the two kinds of polyporphine film (Fig. 4 left). In fact, pCoP-I gives a high and thin peak (398.1 eV) accompanied by a satellite peak (401.8 eV) characteristic of such metalated porphyrins.[52] As previously explained,[34] this result testifies the right Co(II) insertion in the porphine units in all the material. In pCoP-II, the N 1s signal is appearing larger than in pCoP-I which seems to indicate a new peak grown up around 400 eV. The modelling of this experimental spectrum has been performed (Fig. 4 right). The best fit between the calculated and real data is obtained assuming that some of the porphyrins have been transformed in the free base form (29%) while the others (71%) have remained metalated.

As precedently established,[35] this additional feature could possibly come from a partial Co(II) cation loss in the polyporphine film during pCoP- II synthesis. In fact, each newly formed *β-β* bond releases two protons thus increasing the local acidity. Due to this high acidity level, the Co(II) cation is replaced by two protons in some of the porphine units as illustrated in Scheme 3.

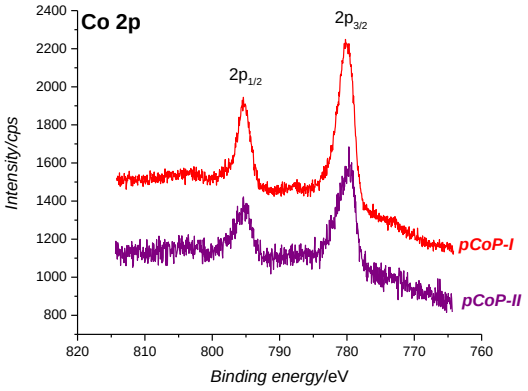

Fig. 3. XPS spectra (spot 100 µm, 25 W, 15 kV, pass energy: 58.7 eV) obtained in Co 2p energy region for pCoP-I (red curve) and pCoP-II (purple curve).

NJC

PAPER

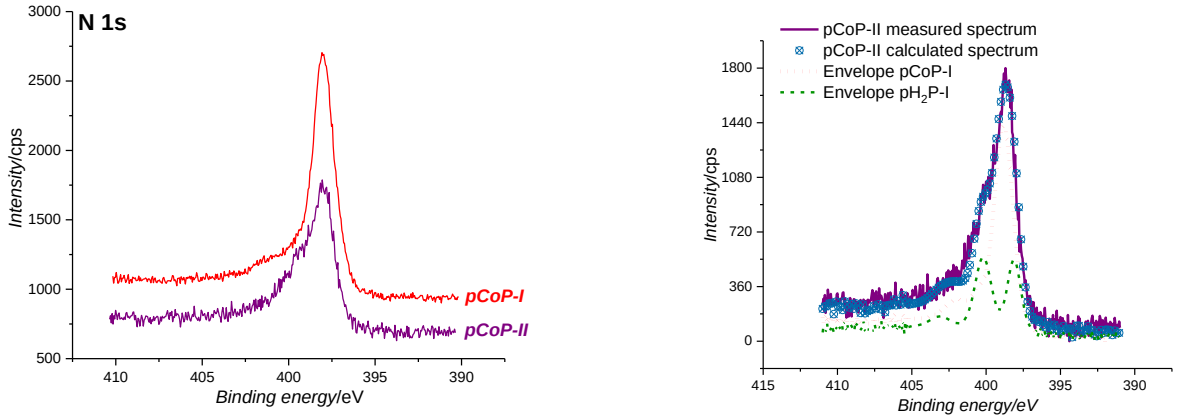

Fig. 4. (left) XPS spectra (spot 100 µm, 25 W, 15 kV, pass energy: 58.7 eV) obtained in N 1s energy region for pCoP-I (red curve) and pCoP-II (purple curve). (right) Decomposition of the pCoP-II N 1s raw signal into its basic components. Purple continuous line: experimentally measured spectrum of the pCoP-II material; blue dots: re-calculated spectrum obtained from linear interpolation of pCoP-I (red plotted curve) and pH_2P-I (green dashed curve) spectra

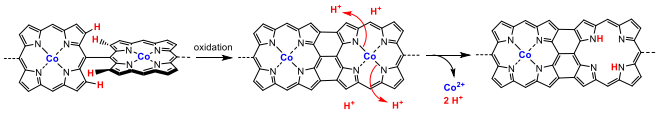

Scheme 3. Plausible mechanism for the demetalation process occurring during pCoP-II formation.

Table 2. Theoretical and XPS measured atom ratio in pCoP-I and pCoP-II.

	Element	Theoretical atom ratio	Measured atom ratio
pCoP-I	C	20	20.9 ± 0.1
	N	4	*4.0 (reference)*
	Co	1	**1.0 ± 0.1**
pCoP-II	C	20	20.9 ± 0.1
	N	4	*4.0 (reference)*
	Co	1	**0.87 ± 0.1**

The C, N and Co atom ratios were deduced from the peak intensities in the XPS spectra. The according results are gathered in Table 2.

As initial basis, the number of N atoms was fixed at 4 (established number for a single porphine unit). For pCoP-I, the resulting calculated numbers of C and Co atoms are in good agreement with the proposed formulae. For pCoP-II the slight defect in cobalt (0.87 instead of 1) confirms the partial loss of cobalt(II) occurring by acidolysis in the course of the cross-linking process.

pCoP-II stability in water and capability to catalyze sulphite oxidation

As the cobalt polyporphine material was designed for sensing sulphite in water, the next step was to study its voltammetric behavior and stability over potential cycling in this kind of medium. Therefore, the modified electrode was introduced in an aqueous solution containing 0.1 M $NaNO_3$ under an argon atmosphere and was then submitted to ten successive potential scans between -1.40 and 0.85 V. The resulting voltammetric recording is presented in Fig. 5.

In Fig. 5, the two reversible systems O1/R1 and R2/02 are observed at 0.25 and -1.0 V (position of peaks O1 and R2, respectively; see Table 3). By comparing with the response in acetonitrile (see above) and in accordance with our previously

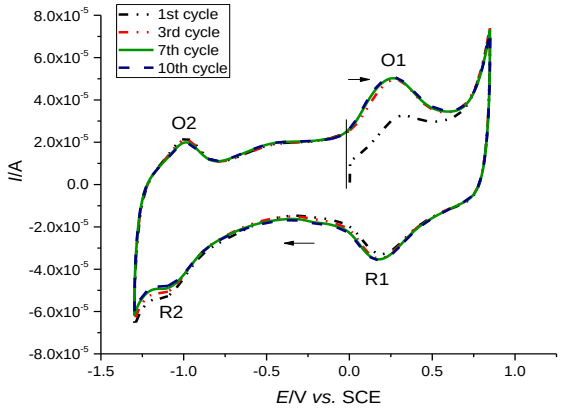

Fig. 5. Cyclic voltammograms obtained for 10 successive cycles in aqueous solution of $NaNO_3$ 0.1 M (v = 0.1 V.s^{-1}) of pCoP-II polyporphine film deposited on GC disc.

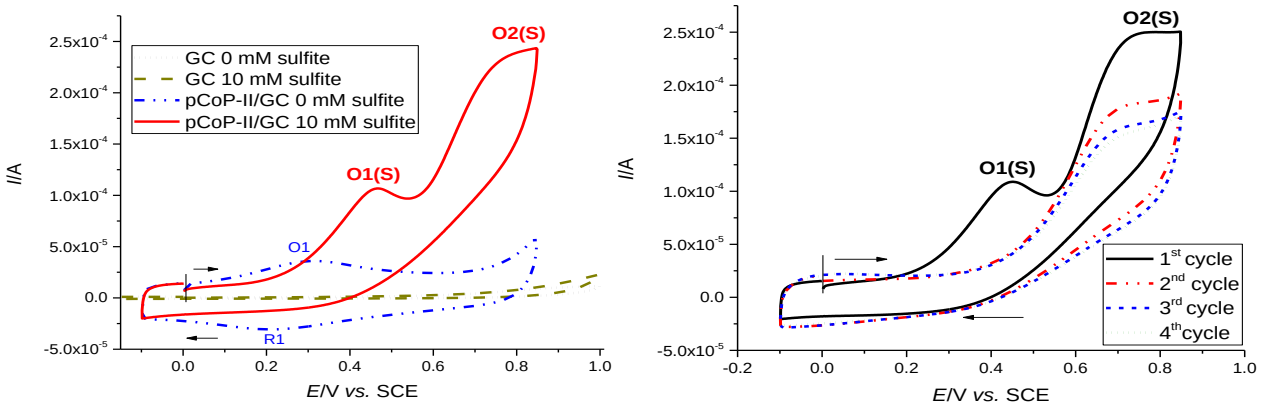

Fig. 6. (left) Cyclic voltammograms obtained in 0.1 M $NaNO_3$ in distilled water on GC or on pCoP-II/GC modified electrode in the absence and in the presence of 10 mM of sulphite (v = 0.1 V.s^{-1}). (right) Multiple-sweep voltammogram of pCoP-II/GC modified electrode in a 10 mM sulphite solution ($NaNO_3$ 0.1 M, v = 0.1 V.s^{-1})

Table 3. Relevant parameters for 10th cycle's peaks displayed on Fig. 5 (films deposited on GC disk, $NaNO_3$ 0.1 M, v = 0.1 V.s^{-1})

	Characteristics signal	O1	02	R1	R2
pCoP-II (10th cycle)	Peak potential (V)	0,25	-0.99	0,18	-1.1
	Charge (µC)	6.6	*N.D.*	6.5	*N.D.*
	Peak intensity (µA)	50.8	19.4	-35.7	-47.2
	Peak intensity variation in 9 cycles (%)	+2.0	-5.8	+2.3	-7.6

reported work,[34] these systems can be attributed to the electron transfer reactions of the Co(II)/Co(III) and Co(I)/Co(II) redox couples. Moreover, as shown in Table 3, the variation of the current response is insignificant between the second and the tenth cycle (individual voltammograms appearing superimposed in Fig. 5). From these observations, the stability of pCoP-II was estimated satisfactory for sulphite detection.

Fig. 6 provides the cyclic voltammograms (CV) of the pCoP-II modified electrode in water containing 0.1 M $NaNO_3$ before and after addition of 10 mM of sulphite (as the sodium salt). For comparison the two CV in identical conditions but on a pure glassy carbon (GC) working electrode are also included.

As shown in Fig. 6 (left), with pCoP-II as electrode material, the addition of sulphite causes the appearance of two massive anodic peaks, O1(S) and O2(S), at respectively 0.46 and 0.79 V (peak potentials). The increase in current induced by sulphite addition is 2.5 times larger at O2(S) (+198.4 µA) than at O1(S) (+78.6 µA). Conversely, on the pure GC electrode, no significant evolution of the voltammogram is noted by sulphite addition. Thus the ability of pCoP-II to catalyze sulphite oxidation is demonstrated. In our case, the occurrence of two signals, e. g. O1(S) and O2(S), is quite surprising since just one is generally observed for this sole electrode reaction.[31] Indeed, at the working pH (≈ 9.7), sulphite exists exclusively under the form of SO_3^{2-}.[2, 9, 10]

In order to elucidate this particular feature other conditions were tested for the voltammetric analysis. First of all, the voltammetry was operated in a multi sweep mode (in the case of Fig. 6 (right), same potential scan applied four times successively). In this situation O1(S) is only present in the first anodic scan and disappears thereafter. Simultaneously, O2(S) does just undergo a slight decrease from scan to scan. Furthermore, O1(S) is regenerated if the cell solution is homogenized between two CV scans.

The evolution of the cyclic voltammogram as a function of the scan rate was also studied. Fig. 7 presents the CV of a pCoP-II modified electrode in contact with a 4.5 mM sulphite aqueous solution for which the scan rate was varied from 25 to 125 mV/s by step of 25 mV/s. As obtained from the resultant recordings, the peak currents for both O1(S) and O2(S) were plotted against the square root of scan rate (Fig. 8, left) or the scan rate as such (Fig. 8, right).

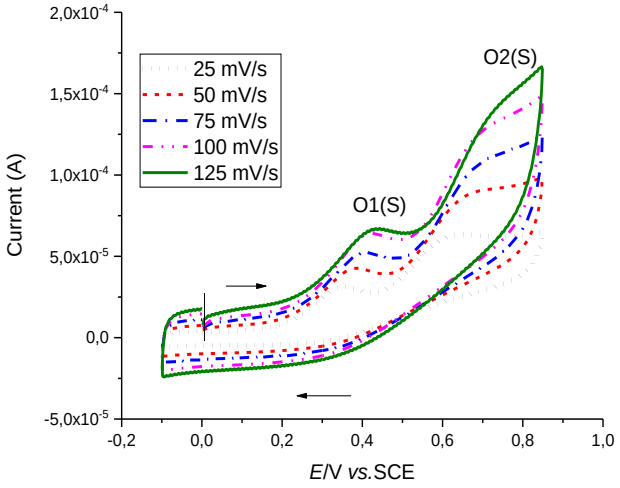

Fig. 7. Voltammograms obtained with a pCoP-II modified electrode in a 4.5 mM sulphite aqueous solution (0.1 M $NaNO_3$ in distilled water) at different scan rates.

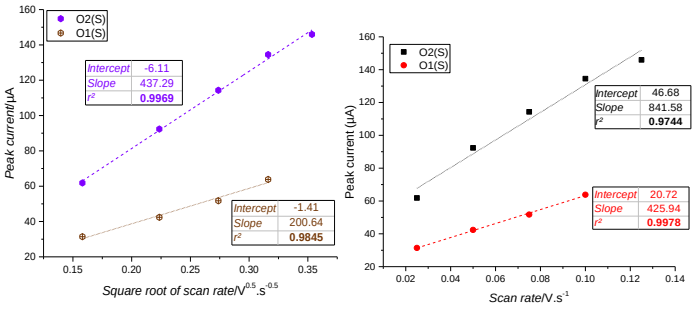

Fig. 8. Plots of O1(S) and O2(S) peak currents as a function of the scan rate (right) or the square root of the scan rate (left).

Concerning O2(S), the best agreement with a linear plot is vs. $v^{1/2}$ (r^2=0.9969), which is in accordance with the current limited by the sulphite ions diffusion in solution.[53, 54] On the contrary, for O1(S), the peak current varies linearly but vs. v, that is typical of electroactive species immobilized on the electrode surface.[53, 54] As a possible explanation, we propose that O1(S) concerns specifically the sulphite ions which have diffused into the polymer film before initiation of the voltammetric scans. This diffusion is slow as compared to what occurs in solution.

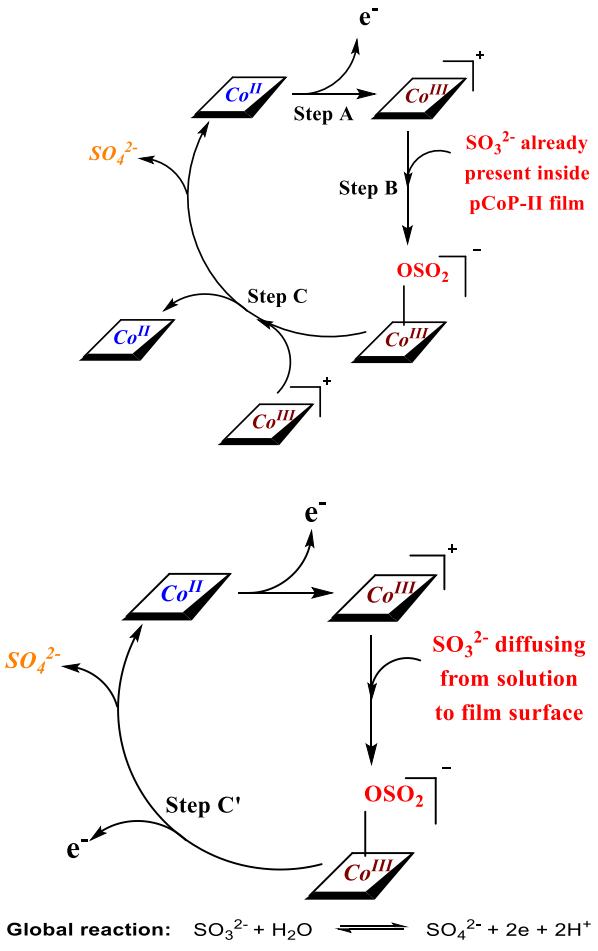

Scheme 4. Proposed reaction mechanisms operating either at O1(S) (left) or O2(S) (right) and global reaction (bottom).

Therefore, this part of sulphite initially present in the porous structure of pCoP-II couldn't be renewed in the period of time available during the voltammetric experiment explaining that O1(S). is only expressed in the first potential scan and not in the following ones. Two distinct mechanisms should be considered operating either at O1(S) or O2(S): both are presented in Scheme **4**.

First of all, it should be specified that SO_3^{2-} is expected to be oxidized in SO_4^{2-} which requires the transfer of two electrons.[22, 30, 55] For the process operating at O1(S) (left of Scheme 4), the catalytic cycle begins by oxidation of Co(II) in Co(III) at the center of the porphyrin macrocycles (step A). Afterwards the coordination of SO_3^{2-} (favored at the +III oxidation state) takes place at the axial position of the porphyrin leading to the formation of an adduct complex (step B). Notably these two first steps have already been described in the cobalt(III) catalyzed auto-oxidation of sulphite in which oxygen serves as the oxidant.[56-58] Continuing the cycle, to account for the second electron transferred, the sulphite adduct complex should interact with another cobalt(III) porphyrin (step C). Although we have no real evidence of this reaction, the cooperation of two redox-active cobalt porphyrins in multiple electron transfer to a single molecule has many precedents: this cooperation can be intra- or intermolecular whether the two cobalt atoms belong to a unique or two different complexes.[59-63] In the pCoP-II material, this cooperation could be facilitated by the proximity and high density of Co(III) electron acceptors available in the volume of this porphyrin network. Conversely, at O2(S), the reaction is localized at the electrode surface and step C would not operate anymore. As an alternate pathway, the oxidation of the sulphite adduct complex proceeds directly through heterogeneous electron transfer with the electrode (step C', right of Scheme 4), and that occurs at the more positive potential of O2(S).

Response in rotating disk electrode voltammetry

In order to get further information on this mechanism, voltammetric experiments on rotating disk electrodes were attempted. This technique has been used to study the catalyzed oxygen reduction reaction on electrodes modified by cobalt porphine deposition.[64, 65] In electrode processes limited by diffusion, the current response is described by the Koutecky-Levich equation:

$$\frac{1}{i_{lim}} = \frac{1}{i_k} + \frac{1}{0{,}62nFAD^{2/3}\nu^{1/6}C^*} \times \frac{1}{\omega^{1/2}} \qquad (1)$$

In this equation, i_{lim} is the limiting current. The inverse of i_{lim} (practically measured on the plateau of the wave) is a linear function of the square root of the rotation rate $\omega^{1/2}$ (rad/s). *n* is the number of electrons exchanged in the considered redox reaction, *A* the geometric area of the disk electrode (cm^2), *D* the diffusion coefficient of the electroactive species moving in solution (cm^2/s), *v* the cinematic viscosity of the electrolytic medium (taken equal to 0.01 cm^2/s in our case), and *C** the concentration in the bulk of the species (mol/cm^3). Finally, i_k is the kinetic current which is reached when i_{lim} is no more controlled by the diffusion in solution of the electroactive species (high electrode rotation speed) but by the intrinsic rate of the pCoP-II catalyzed sulphite electro-oxidation reaction.[53]

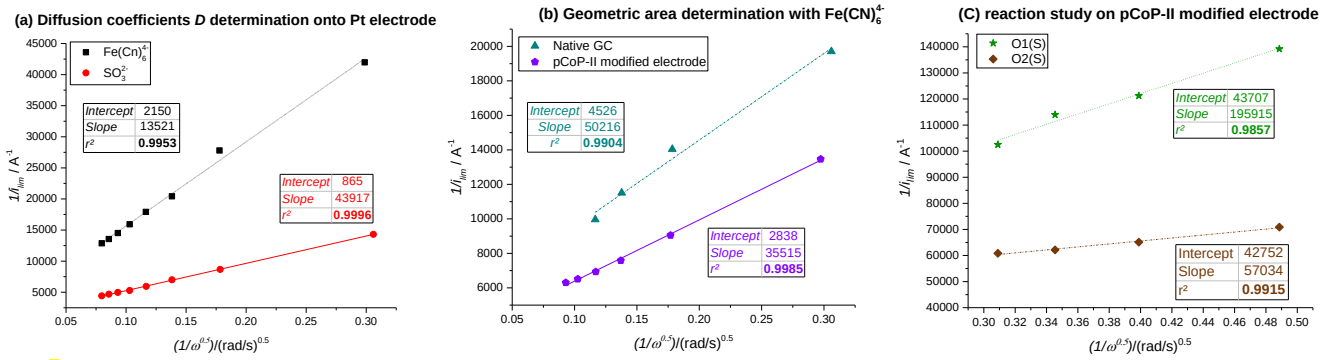

Fig. 9. Koutecky-Levich plots obtained at the different steps of the rotating disk electrode study.

For investigating the sulphite oxidation mechanism on pCoP-II, the Koutecky-Levich plots were performed according a three step procedure. a) First, a platinum disk electrode of known area (3.14 mm²) was used to assess the diffusion coefficient of SO_3^{2-} in our medium. The diffusion coefficient of ferrocyanide as a standard was obtained in similar conditions. b) Then the $[Fe(CN)_6]^{4-}$ probe was employed to determine the geometric area of the native GC and pCoP-II modified electrodes. c) Finally, using the Koutecky-Levich plots, *n*, the number of electrons exchanged in the pCoP-II catalyzed sulphite oxidation reaction was determined on the plateau of both O1(S) and O2(S). The experimental plots are reproduced in Fig. 9 and the resulting data presented in Table 4.

Two observations should be made by considering the results in Table 4. First of all, a significant increase of the geometric area (+33%) is noted between the native GC and the pCoP-II modified electrodes. The reason is that the polymer film overflows out of the initial GC disk onto the surrounding PTFE isolating material, as is also attested by a simple visual examination of the electrode. It demonstrates therefore that the polymer also expands in the horizontal direction with no support of another conductive material. The second point concerns the number of electrons involved in the sulphite oxidation reaction as catalyzed by pCoP- II. Two different cases must be distinguished. At the level of O2(S), the slope of the Koutecky-Levich plot leads to a *n* value of 2, which is in accordance with the predicted reaction.[22, 30, 55] Conversely, the Koutecky-Levich plot issued from the treatment of i_{lim} on the plateau of O1(S) is not ideally linear (r^2 = 0.9856) and the extrapolated slope gives an *n* value of 0.6. It can be concluded that the precedent model does not more apply in which i_{lim} depends exclusively on the diffusion of sulphite ions in solution to move to the electrode surface. Other factors should be considered such as those outlined in the CV study (see above): sulphite ions diffusing into and being oxidized in the volume of the film and participation of the sulphite initially present in this volume.

Table 4. Results issued from exploitation of the Koutecky-Levich plots.

Study (a)	***Species***	**$Fe(CN)_6^{4-}$**	**SO_3^{2-}**
	Diffusion coefficient (cm^2/s)	$4.52*10^{-6}$	$4.72*10^{-6}$
Study (b)	***Electrode type***	**Native GC**	**pCoP-II modified electrode**
	Geometric area (cm^2)	0.09	0.12
Study (c)	***Signal***	**O1(S)**	**O2(S)**
	Number of electrons n	0.6	2.03

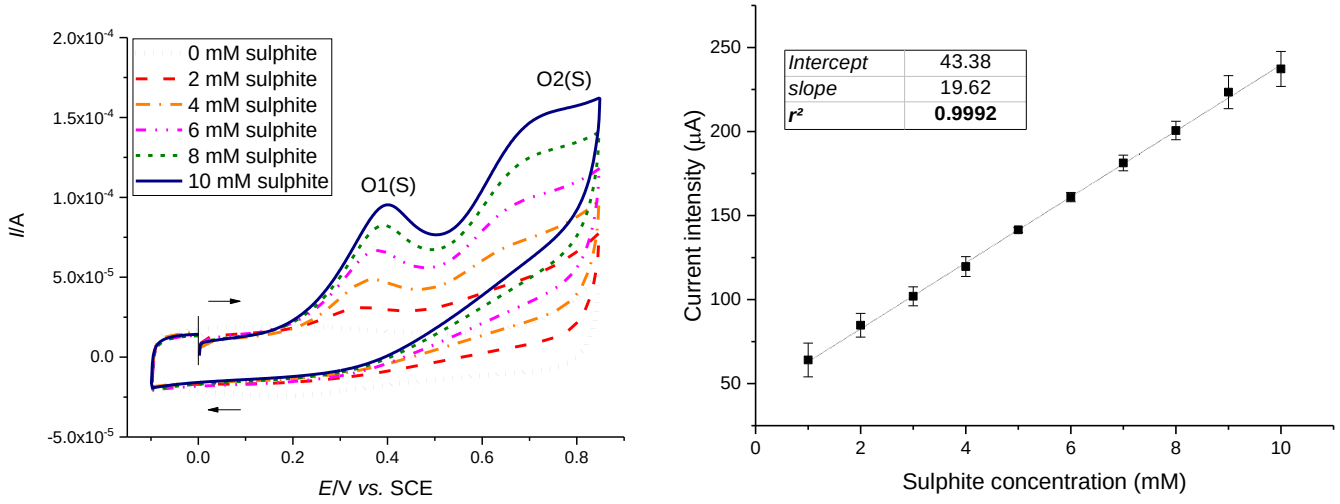

Fig. 10. (left) Cyclic voltammograms obtained on p-CoP-II film (thickness: ca. 100 nm) in 0.1 M $NaNO_3$ aqueous solution (*v* = 0.1 V/s) with increasing sulphite concentration. (right) Plot of O2(S) current as a function of sulphite concentration.

Table 5. Main parameters deduced from the sulphite calibration graph shown in Fig. 10.

parameter	Slope (µA/mM)	Intercept (µA)	R^2	LOD (mM)	LOQ (mM)
value	19.62	43.38	0.9991	0.195	0.649

Capability as a sulphite sensor

In order to evaluate the capacity of pCoP-II for sulphite detection, the electrode response was tested in presence of increasing sulphite concentrations. For each concentration level the current intensity was sampled on peak O2(S) at E_W = +0.75 V vs. SCE. Statistical tests were realized using the method reported by M. Feinberg *et al.*.[66] In accordance with this procedure, the measurements were conducted with 3 different pCoP-II films and ten levels of sulphite concentration (0 to 10 mM) in $NaNO_3$ 0.1 M aqueous solution. All the experiments were performed under Ar atmosphere. The linearity interval was evaluated using the r^2 value. The Limit Of Detection (LOD) and Limit Of Quantification (LOQ) were calculated with the 3σ/slope and 10σ/slope methods respectively.[66]

As shown in Figure 10 and Table 5, the plot O2(S) current=f(sulphite concentration) is linear (r^2=0.9991) between 1 and 10 mM. The LOD is estimated at 0.195 mM. This value is nearly in the same range as with a Co(II) porphyrin based similar system in conditions similar to ours and for which the LOD was found equal to 0.385 mM.[31]

In any case, this result, which has still to be optimized, demonstrates the ability of our system for sensing sulphite in water.

Conclusion and perspective.

A new kind of conducting polymer, designed as cobalt(II) polyporphine of type II (pCoP-II), was synthesized in a straightforward fashion from oxidative reticulation of the type I form. The whole of spectroscopic data indicate that the porphyrin structure remains intact during this transformation. In the course of the electrode reaction, a marginal portion of the Co(II) porphyrin macrocycles undergoes demetalation through acidolysis.

The pCoP-II polymer exhibits a stable electrochemical response in aqueous medium. This material catalyzes the electrooxidation of sulphite making it operative for sensing this substance in water. The capacities of the according modified electrode should be improved in many ways. The most promising ones which will be pursued in the next future will aim at the enhancement of the electrode specific area (for example by changing the GC supporting material with carbon nanotubes or graphene), the increase of the signal-to-noise ratio by the use of a better performing voltammetric method (differential pulse or square wave voltammetry instead of the classical linear sweep mode), or the generation of a more intense signal by forcing sulphite mass transfer to the electrode (for example by the means of a rotating disk electrode).

Conflicts of interest

There are no conflicts of interest to declare.

Acknowledgement

Financial supports from CNRS, University of Bourgogne Franche Comté, Conseil Régional de Bourgogne (PhD grant JCE for S.D.R.), European Union and Conseil Régional de Bourgogne FABER programs are acknowledged (S.D.R., C.H.D., D.L., F.H., O.H.). C.H.D. thanks the CNRS for granting him the opportunity to work as a full time researcher for one year ("délégation CNRS", Sept. 2015). C. H. D., D. L. and S. D. R. are grateful to Dr. P. Richard and IOC company, especially I. Cattier and H. Gibault, for their interest in this research.

References

1. L. F. Green, *Food Chem.*, 1976, **1**, 103-124.
2. P. Ribéreau-Gayon, D. Duboudieu, B. Donèche, A. Lonvaud and G. De Revel, *Traité d'oenologie. Microbiologie du vin, vinifications*, Dunod, Paris, 7th edn., 2017.
3. S. L. Taylor, N. A. Higley and R. K. Bush, *Adv. food res.*, 1986, **30**, 1-76.
4. R. K. Bush, S. L. Taylor and W. Busse, *J. Allergy Clin. Immunol.*, 1986, **78**, 191-202.
5. A. F. Gunnison, D. W. Jacobsen and H. J. Schwartz, *Crit. rev. toxicol.*, 1987, **17**, 185-214.
6. D. W. Roberts, D. Basketter, I. Kimber, J. White, J. McFadden and I. R. White, *Contact dermatitis*, 2012, **66**, 123-127.
7. H. Vally, N. L. Misso and V. Madan, *Clin. Exp. Allergy*, 2009, **39**, 1643-1651.
8. H. Vally and P. J. Thompson, *Addiction biology*, 2003, **8**, 3-11.
9. J. Blouin and J. Cruège, *Analyse et composition des vins* Dunod, Paris, 2nd edn., 2013.
10. C. Bonder, *Analyses et décisions en oenologie, guide pratique du laboratoire et de la cave*, Lavoisier, Paris, 2014.
11. X.-W. Wang, J.-F. Liu, X.-Y. Wang, B. Shao, L.-P. Liu and J. Zhang, *Anal. Methods*, 2015, **7**, 3224-3228.
12. M. Koch, R. Koppen, D. Siegel, A. Witt and I. Nehls, *J. Agric. Food. Chem.*, 2010, **58**, 9463-9467.
13. K. Yoshikawa, Y. Uekusa and A. Sakuragawa, *Food Chem.*, 2015, **174**, 387-391.
14. G. Jankovskiene, Z. Daunoravicius and A. Padarauskas, *J. Chromatogr. A*, 2001, **934**, 67-73.
15. M. Masár, M. Danková, E. Ölvecká, A. Stachurová, D. Kaniansky and B. Stanislawski, *J. Chromatogr. A*, 2005, **1084**, 101-107.
16. H. K.-M. Ali A. Ensafi, *Int. J. Electrochem. Sci.*, 2010, **5**, 392-406.
17. M. Amatatongchai, W. Sroysee, S. Chairam and D. Nacapricha, *Talanta*, 2015, **133**, 134-141.
18. P.-Y. Chen, Y.-M. Chi, H.-H. Yang and Y. Shih, *J. Electroanal. Chem.*, 2012, **675**, 1-4.
19. T. R. L. Dadamos and M. F. S. Teixeira, *Electrochim. Acta*, 2009, **54**, 4552-4558.
20. J. B. Raoof, R. Ojani and H. Karimi-Maleh, *Int. J. Electrochem. Sci.*, 2007, **2**, 257-269.
21. B. Molinero-Abad, M. A. Alonso-Lomillo, O. Domínguez-Renedo and M. J. Arcos-Martínez, *Anal. Chim. Acta*, 2014, **812**, 41-44.

22. O. Ordeig, C. E. Banks, F. J. del Campo, F. X. Muñoz, J. Davis and R. G. Compton, *Electroanalysis*, 2006, **18**, 247-252.
23. R. Rawal and C. S. Pundir, *Int. J. Biol. Macromol.*, 2012, **51**, 449-455.
24. A. Safavi, N. Maleki, S. Momeni and F. Tajabadi, *Anal. Chim. Acta*, 2008, **625**, 8-12.
25. I. Streeter, A. J. Wain, J. Davis and R. G. Compton, *J. Phys. Chem. B*, 2005, **109**, 18500-18506.
26. P. D. Tzanavaras, E. Thiakouli and D. G. Themelis, *Talanta*, 2009, **77**, 1614-1619.
27. Y. Yang, Y. Yan, X. Chen, W. Zhai, Y. Xu and Y. Liu, *Electrocatalysis*, 2014, **5**, 344-353.
28. S.-M. Chen, *J. Mol. Catal. A: Chem.*, 1996, **112**, 227-285.
29. J. P. Muena, M. Villagrán and M. J. Aguirre, *Int. J. Electrochem. Sci.*, 2013, **8**, 621-633.
30. G. Ramírez, M. C. Goya, L. Mendoza, B. Matsuhiro, M. Isaacs, Y. O. Y. Chen, M. C. Arévalo, J. Henríquez, W. Cheuquepán and M. J. Aguirre, *J. Coord. Chem.*, 2009, **62**, 2782-2791.
31. R. Arce, J. Romero and M. J. Aguirre, *J. Appl. Electrochem.*, 2014, **44**, 1361-1369.
32. J. H. Vélez, J. P. Muena, M. J. Aguirre, G. Ramirez and F. Herrera, *Int. J. Electrochem. Sci.*, 2012, **7**, 3167-3177.
33. B. Pazv, C. Yo-Ying, R. Galo, J. C. Maria, M. Betty, Leonora Mendoza, Mauricio Isaacs, Macarena García, M. C. Arevalo and M. J. Aguirre, *Collect. Czech. Chem. Commun.*, 2009, **74**, 545-557.
34. S. D. Rolle, D. V. Konev, C. H. Devillers, K. V. Lizgina, D. Lucas, C. Stern, F. Herbst, O. Heintz and M. A. Vorotyntsev, *Electrochim. Acta*, 2016, **204**, 276-286.
35. M. A. Vorotyntsev, D. V. Konev, C. H. Devillers, I. Bezverkhyy and O. Heintz, *Electrochim. Acta*, 2011, **56**, 3436-3442.
36. D. K. Dogutan, M. Ptaszek and J. S. Lindsey, *J. Org. Chem.*, 2007, **72**, 5008-5011.
37. C. H. Devillers, A. K. D. Dimé, H. Cattey and D. Lucas, *C. R. Chim.*, 2013, **16**, 540-549.
38. D. V. Konev, C. H. Devillers, K. V. Lizgina, V. E. Baulin and M. A. Vorotyntsev, *J. Electroanal. Chem.*, 2015, **737**, 235-242.
39. D. V. Konev, K. V. Lizgina, D. K. Khairullina, M. A. Shamraeva, C. H. Devillers and M. A. Vorotyntsev, *Russ. J. Electrochem.*, 2016, **52**, 778-787.
40. S. Cosnier, C. Gondran, K. Gorgy, R. Wessel, F.-P. Montforts and M. Wedel, *Electrochem. Commun.*, 2002, **4**, 426-430.
41. S. Cosnier, C. Gondran, R. Wessel, F.-P. Montforts and M. Wedel, *J. Electroanal. Chem.*, 2000, **488**, 83-91.
42. S. Gottesfeld, A. Redondo, I. Rubinstein and S. W. Feldberg, *J. Electroanal. Chem.*, 1989, **265**, 15-22.
43. M. A. Vorotyntsev, M. Skompska, E. Pousson, J. Goux and C. Moise, *J. Electroanal. Chem.*, 2003, **552**, 307-317.
44. J. Yang, Y. Yang, J. Hou, X. Zhang, W. Zhu, M. Xu and M. Wan, *Polymer*, 1996, **37**, 793-798.
45. K. M. Kadish, E. V. Caemelbecke and G. Royal, in *The Porphyrin Handbook* eds. K. M. Kadish, K. M. Smith and R. Guilard, 2000, vol. 8, ch. 55, pp. 61-69.
46. M. A. Vorotyntsev, D. V. Konev, C. H. Devillers, I. Bezverkhyy and O. Heintz, *Electrochim. Acta*, 2010, **55**, 6703-6714.
47. O. P. Charkin and N. M. Klimenko, *Russ. J. Inorg. Chem.*, 2013, **58**, 1058-1069.
48. K. L. Eriksson, W. W. Chow, C. Puglia, J. E. Backvall, E. Gothelid and S. Oscarsson, *Langmuir*, 2010, **26**, 16349-16354.
49. K. Flechtner, A. Kretschmann, H.-P. Steinrück and J. M. Gottfried, *J. Am. Chem. Soc.*, 2007, **129**, 12110-12111.
50. A. Gulino, P. Mineo and I. Fragalà, *Inorg. Chim. Acta*, 2008, **361**, 3877-3881.
51. Z. Sun, J. Li, H. Zheng, X. Liu, S. Ye and P. Du, *Int. J. Hydrogen Energy*, 2015, **40**, 6538-6545.
52. R. G. Hayes and S. Muralidaharan, *J. Am. Chem. Soc.*, 1980, **102**, 5107-5108.
53. A. J. Bard and L. R. Faulkner, *Electrochimie. Principes, méthodes et applications*, Masson, Paris, 1983.
54. C. Costentin and J. M. Saveant, *Phys. Chem. Chem. Phys.*, 2015, **17**, 19350-19359.
55. A. Isaac, J. Davis, C. Livingstone, A. J. Wain and R. G. Compton, *Trends Anal. Chem.*, 2006, **25**, 589-598.
56. C. Brandt and R. Van Eldik, *Chem. Rev.*, 1995, **95**, 119-190.
57. V. K. Joshi, R. Van Eldik and G. M. Harris, *Inorg. Chem.*, 1986, **25**, 2229-2237.
58. R. Van Eldik, N. Coichev, K. Bal Reddy and A. Gerhard, *Ber. Bunsen-Ges. Phys. Chem*, 1992, **96**, 478-481.
59. J. P. Collman, P. S. Wagenknecht and J. E. Hutchison, *Angew. Chem., Int. Ed. Engl.*, 1994, **33**, 1537-1554.
60. W. Jentzen, I. Turowska-Tyrk, W. R. Scheidt and J. A. Shelnutt, *Inorg. Chem.*, 1996, **35**, 3559-3567.
61. C. Shi, B. Steiger, M. Yuasa and F. C. Anson, *Inorg. Chem.*, 1997, **36**, 4294-4295.
62. B. S. Sudhindra and J. H. Fuhrhop, *Int. J. Quantum Chem.*, 1981, **20**, 747-753.
63. L. E. Webb and E. B. Fleischer, *J. Am. Chem. Soc.*, 1965, **87**, 667-669.
64. A. Marín, M. J. Aguirre, J. P. Muena, W. Dehaen, W. Maes, T. H. Ngo, G. Ramírez and M. C. Arévalo, *Int. J. Electrochem. Sci.*, 2015, **10**, 3949-3960.
65. S. Yoshimoto, J. Inukai, A. Tada, T. Abe, T. Morimoto, A. Osuka, H. Furuta and K. Itaya, *J. Phys. Chem. B*, 2004, **108**, 1948-1954.
66. M. Feinberg and G. Lamarque, *Tech. Ing., Anal. Caract.*, 2005, **P152**, P226/221-P226/220.